

Supplementary Information

Ultrafine Ir Nanoclusters on Manganese Dioxide for pH-Universal Oxygen Evolution Reactions and Rechargeable Zinc-Air Batteries

Zhe Liu,^a Yonggang Liu,^a Shilong Liu,^a Sanchuan Liu,^a Yujun Tang,^a and Zhenghua Tang^{*,a,b}

^a Guangzhou Key Laboratory for Surface Chemistry of Energy Materials and New Energy Research Institute, School of Environment and Energy, South China University of Technology, Guangzhou Higher Education Mega Centre, Guangzhou, 510006, China.

E-mail: zhht@scut.edu.cn.

^b State Key Laboratory of Subtropical Building Science, South China University of Technology, Guangzhou, 510640, China

Table S1. The element content determined by XPS measurement of 3%-Ir-MnO₂, 5%-Ir-MnO₂ and 8%-Ir-MnO₂.

Catalyst	Ir (at. %)	Mn (at. %)	O (at. %)
3%-Ir-MnO ₂	1.75	26.75	71.50
5%-Ir-MnO ₂	2.86	22.14	75
8%-Ir-MnO ₂	5.70	21.20	73.10

Table S2. Fitting parameters obtained from the EIS data of x%-Ir-MnO₂ and IrO₂ for OER at different pH window.

<i>Neutral</i>	R _s (Ω)	R _{ct} (Ω)	W1-R	W1-T	W1-P	CPE1-T	CPE1-P
5%-Ir-MnO ₂	15.3	31.6	7.3	4.7	0.75	0.06	0.61
3%-Ir-MnO ₂	13.9	37	9.8	3.2	0.76	0.055	0.62
8%-Ir-MnO ₂	15	40.5	10	2.5	0.33	0.024	0.53
IrO ₂	15	105.6	40	2.8	0.578	0.0371	0.718

<i>Alkaline</i>	R _s (Ω)	R ₁ (Ω)	CPE ₁ -T(F)	CPE ₁ -P	R _{ct} (Ω)	CPE ₂ -T(F)	CPE ₂ -P
5%-Ir-MnO ₂	1.343	2.06	5.22E-06	0.90448	5.995	0.10623	0.78707
3%-Ir-MnO ₂	4.5	0.85	0.024	0.55	15.4	0.015	0.7
8%-Ir-MnO ₂	4	0.8	0.575	0.85	7.55	1.5	0.84
IrO ₂	4.02	0.1	0.003	0.64	38.8	0.013	0.87

<i>Acid</i>	R _s (Ω)	R ₁ (Ω)	CPE ₁ -T(F)	CPE ₁ -P	R _{ct} (Ω)	CPE ₂ -T(F)	CPE ₂ -P
5%-Ir-MnO ₂	2.22	0.955	0.00587	0.6258	4.52	0.044	0.7227
3%-Ir-MnO ₂	4.97	5.5	0.0365	0.348	6.83	0.014	0.77
8%-Ir-MnO ₂	5.6	1.36	0.102	0.669	7.17	0.099	0.856
IrO ₂	2.56	0.5	1.7	0.7	20	0.75	0.81

R_s: electrolyte resistance.

R_1 : solid-electrolyte interface resistance.

R_{ct} : charge-transfer resistance.

CEP_1 : capacitance generated from the Faradic process, and constant-phase element.

CEP_2 : capacitance arisen from the solid-electrolyte interface process.

W1: Warburg Element (short).

Table S3. Exchange current density (mA cm^{-2}) of as synthesized catalysts in different conditions.

	neutral	alkaline	acid
3%-Ir-MnO ₂	0.21	1.40	1.14
5%-Ir-MnO ₂	0.44	3.49	2.28
8%-Ir-MnO ₂	0.3	1.995	1.563
IrO ₂	0.049	0.50	0.81

Table S4. The OER and corresponding ZAB performances comparison between 5%-Ir-MnO₂ and the recently reported similar OER electrocatalysts.

Catalyst	Media	Overpotential (mV) at 10 (mA cm^{-2})	Power density of ZAB (mW cm^{-2})	Capacity of ZAB ($\text{mA h g}_{\text{Zn}}^{-1}$)	Stability of ZAB	Reference
5%-Ir-MnO ₂	0.2 M PBS 1 M KOH 0.5 M H ₂ SO ₄ neutral / alkaline ZABs	330 240 267	216.2	792/ 655.4	200 h / 120 h	This work
RuIrCaO _x	0.5 M KHCO ₃	254	-	-	-	¹

SA-Ir/NC	Neutral ZAB	-	76	776.8	100 h	2
CoIr-0.2	1.0 M PBS	373	-	-	140 h	3
Ir/CoNiB	1 M KOH	178	-	-	-	4
Co-MnO ₂ -O _V	1 M KOH	279	-	-	-	5
SA Ag-MnO ₂	1 M KOH Alkaline ZAB	640	273.2	683.1	107 h	6
MnO/Co/PGC	1 M KOH Alkaline ZAB	301	172	872	350 cycles	7
MnO ₂ -IL _{0.5}	1 M KOH Alkaline ZAB	394	166	745	40 h	8
0.022FeMn	0.1 M KOH Alkaline ZAB	660	30.65	669	20 h	9
24Co-MnO ₂	0.1 M KOH Alkaline ZAB	430	197.7	791.5	162 h	10
Ir np/GF	0.5 M H ₂ SO ₄	290	-	-	-	11
IrTe-NTs	0.1 M HClO ₄ 0.1 M PBS 1 M KOH	290 590 320	-	-	-	12
MnS _{0.10} O _{1.90} / MnCo ₂ S ₄	0.2 M PBS 1 M KOH Alkaline ZAB	414 300	-	746	140 h	13

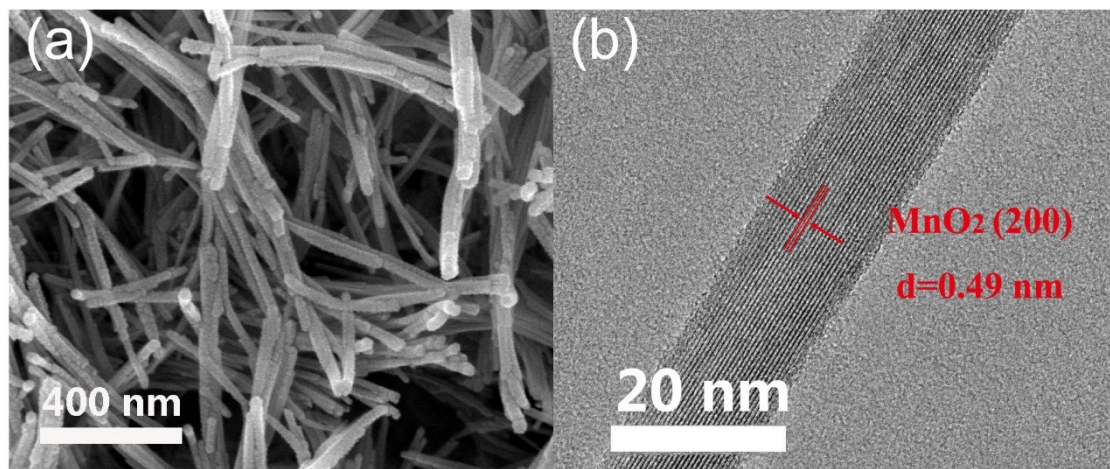


Figure S1. Typical FE-SEM (a) and HR-TEM (b) micrographs of MnO_2 .

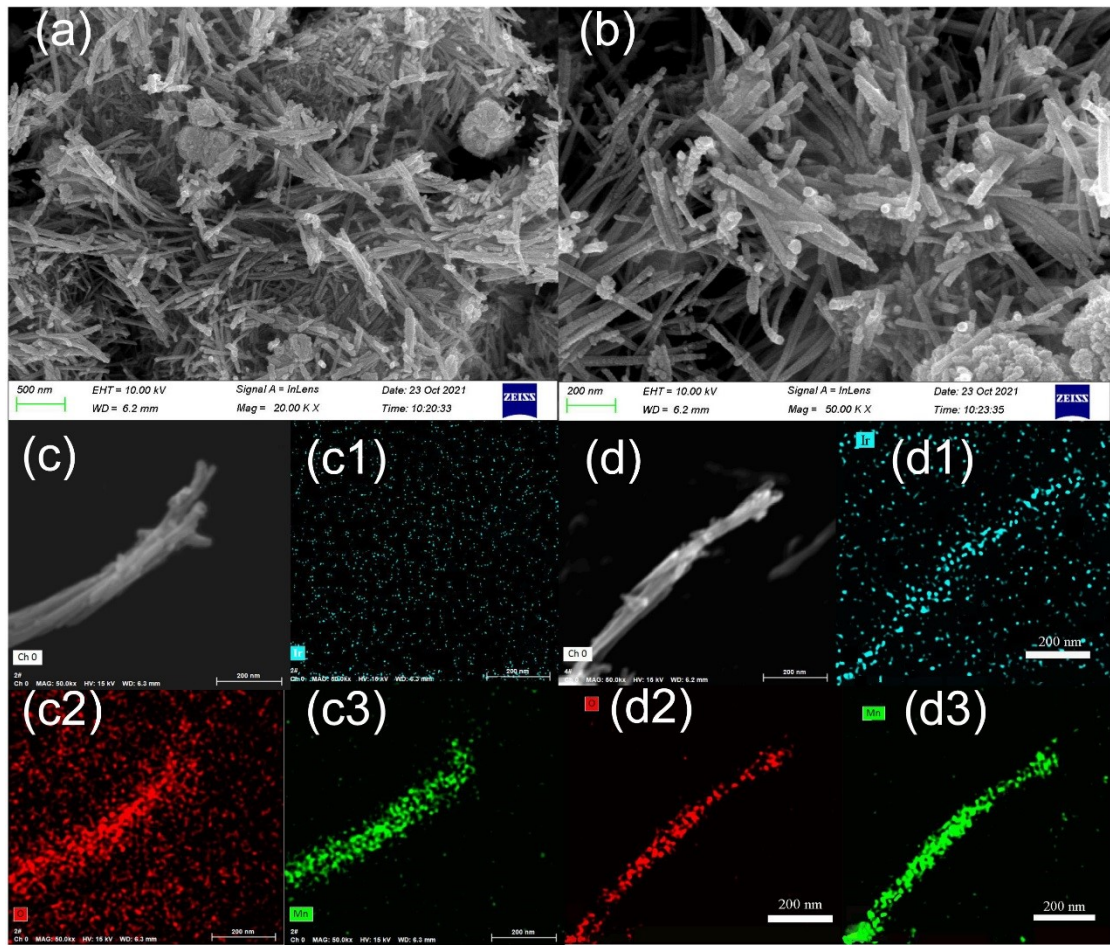


Figure S2. (a), (b) Typical SEM images and (c), (d) element mapping of magnified field of 3%-Ir- MnO_2 and 8%-Ir- MnO_2 .

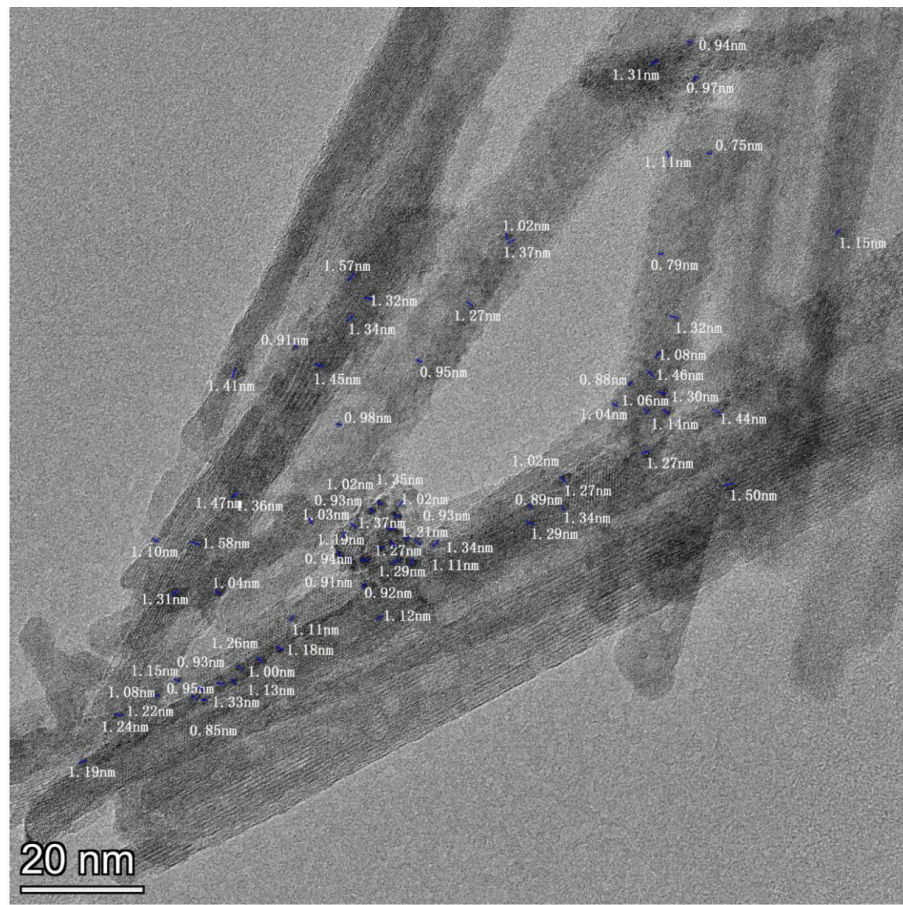


Figure S3. Representative TEM image of the 5%-Ir-MnO₂ with measured size of the marked clusters.

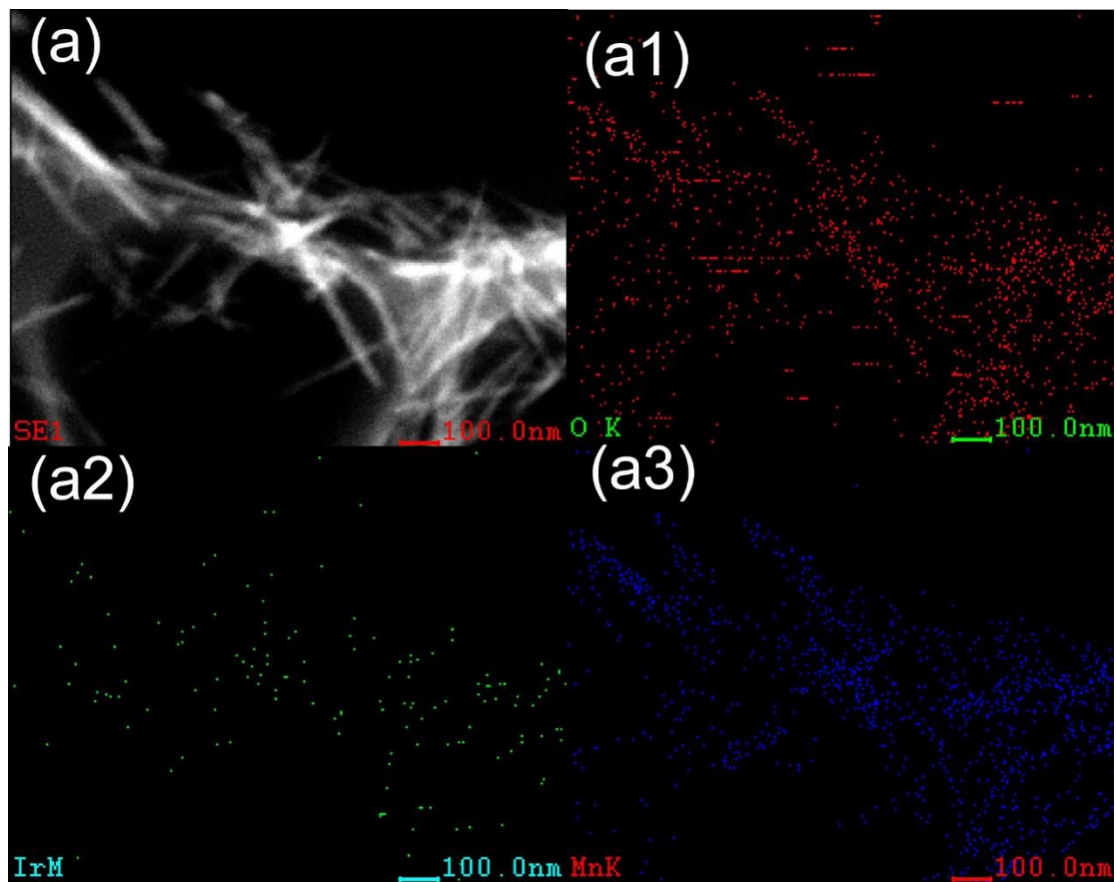


Figure S4. HAADF-STEM image and the corresponding EDS mapping of 5%-Ir-MnO₂.

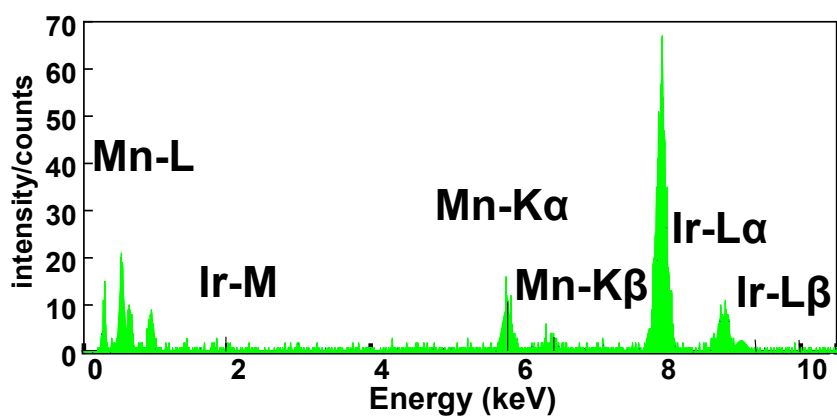


Figure S5. EDS spectrum of the region in Fig. 1e.

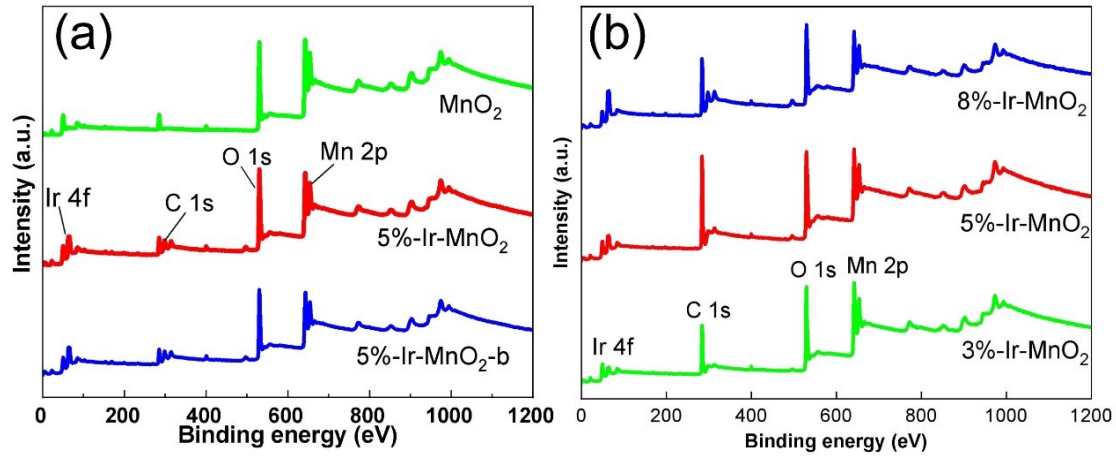


Figure S6. (a) XPS survey-scan spectra of the MnO_2 , 5%-Ir- MnO_2 -b, and 5%-Ir- MnO_2 samples. (b) XPS survey-scan spectra of 3%-Ir- MnO_2 , 5%-Ir- MnO_2 and 8%-Ir- MnO_2 samples.

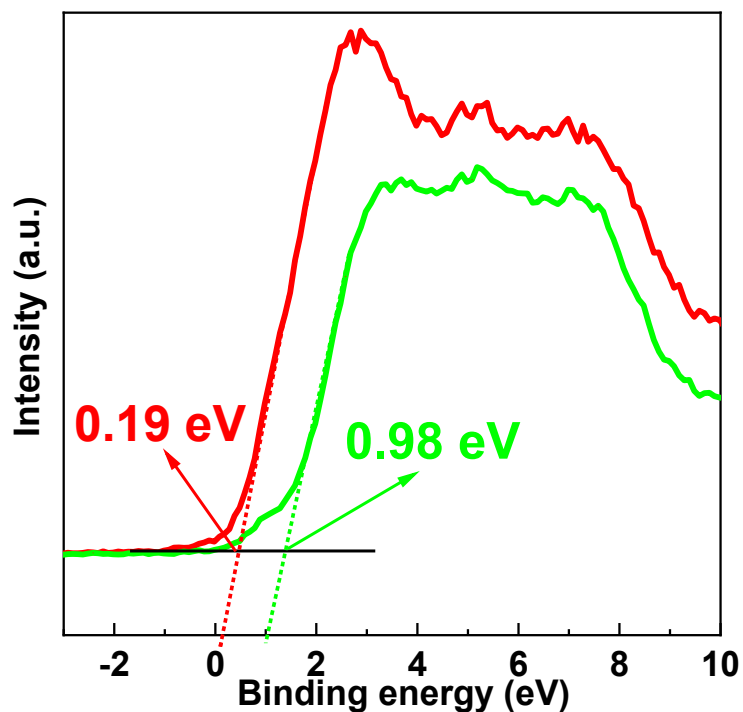


Figure S7. Valence state spectra from XPS test of MnO_2 and 5%-Ir- MnO_2 .

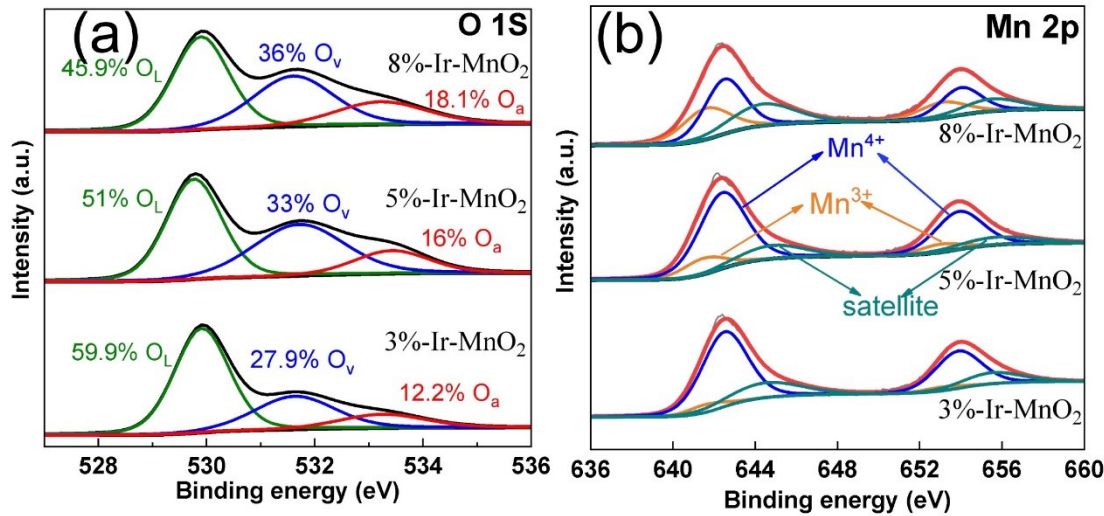


Figure S8. The high-resolution XPS spectra of O 1s (a) and Mn 2p (b) of x%Ir-MnO₂.

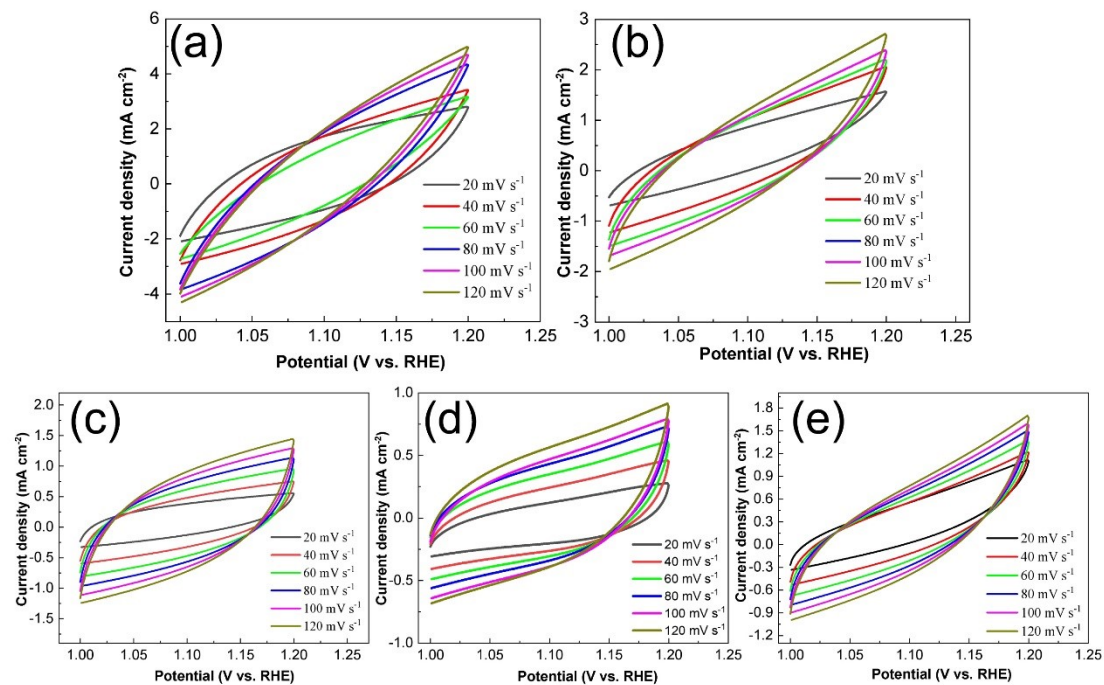


Figure S9. CV curves of 5%-Ir-MnO₂ (a), 3%-Ir-MnO₂ (b), 8%-Ir-MnO₂ (c), MnO₂ (d) and IrO₂ (e) in 0.2 M PBS with different scan rate between 1.0 V and 1.2 V.

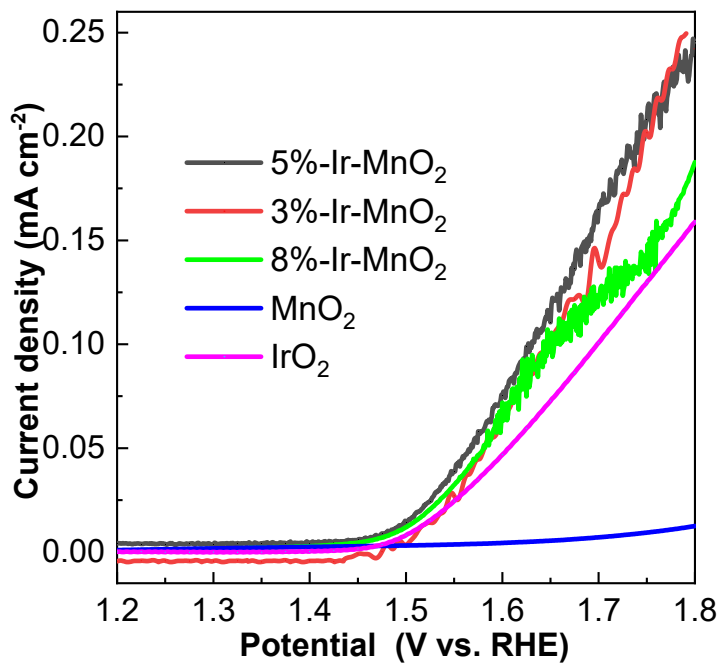


Figure S10. The OER polarization curves of 3%-Ir-MnO₂, 5%-Ir-MnO₂, 8%-Ir-MnO₂, MnO₂, and IrO₂ corrected by ECSA in 0.2 M PBS.

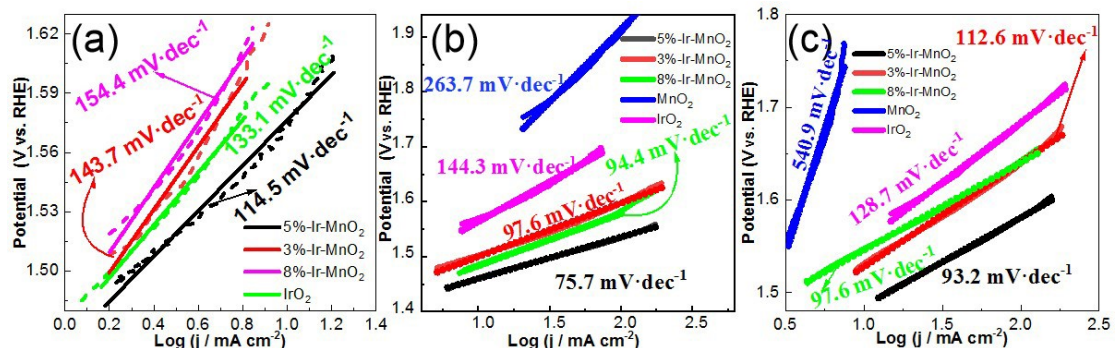


Figure S11. Tafel plots of 3%-Ir-MnO₂, 5%-Ir-MnO₂, 8%-Ir-MnO₂, MnO₂, and IrO₂ in 0.2 M PBS (a), 1 M KOH (b), and 0.5 M H₂SO₄ (c).

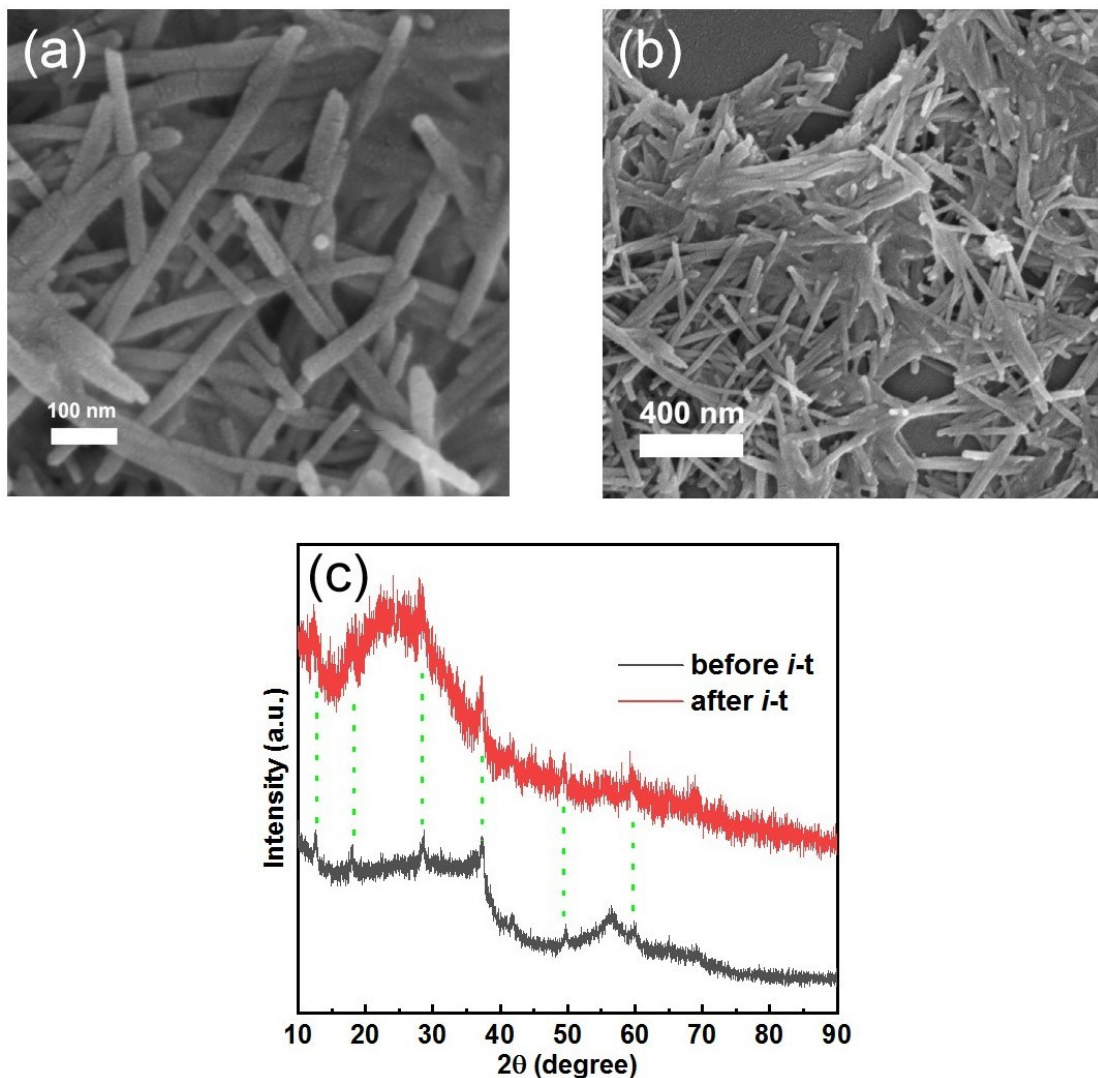


Figure S12. (a, b) SEM images with different magnification of 5%-Ir-MnO₂ after OER *i-t* test in neutral electrolyte. (c) Post-catalytic XRD spectra before and after *i-t* test.

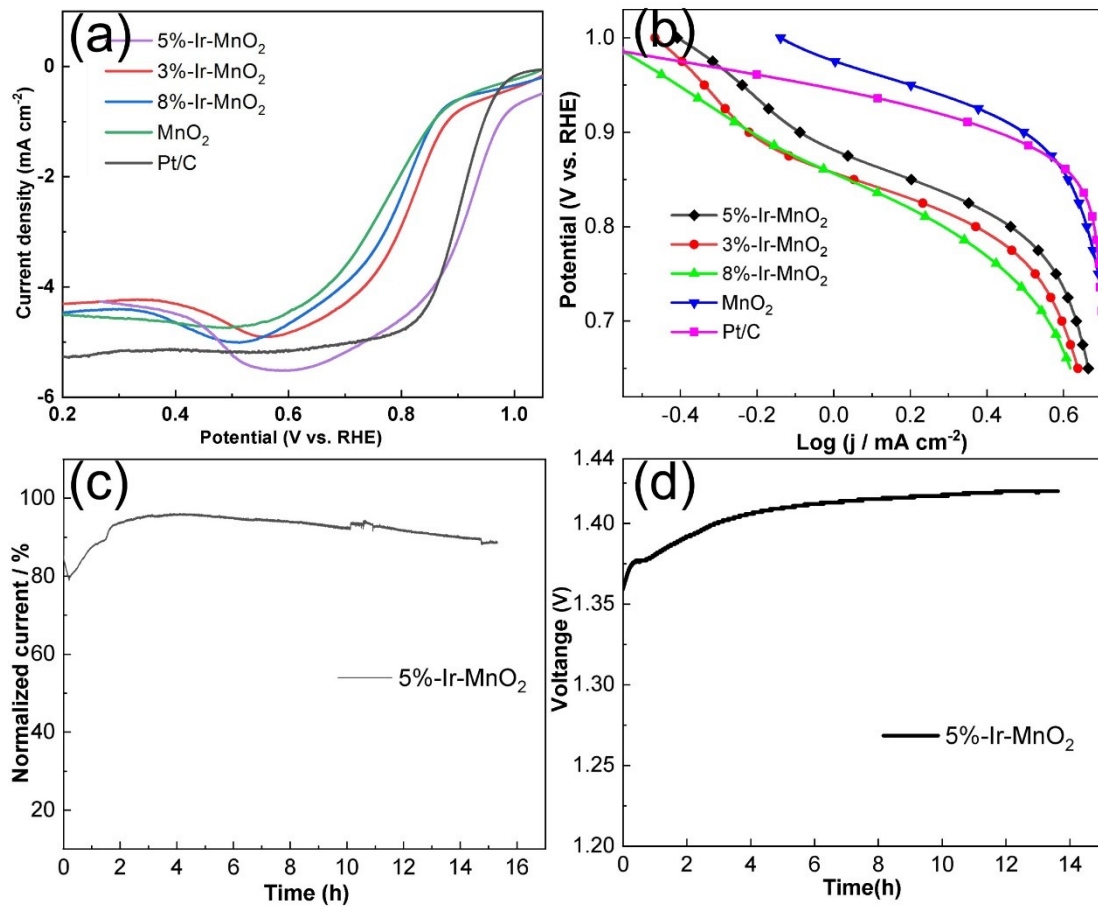


Figure S13. (a) The ORR LSV curves of x-Ir-MnO₂, MnO₂, and Pt/C with a scanning rate of 10 mV s^{-1} at rotating speed of 1600 rpm in 0.1 M KOH, (b) Tafel plots for these catalysts. (c) I-t curve at 0.8 V of 5%-Ir-MnO₂. (d) OCP of Zn-air battery with 5%-Ir-MnO₂ as air electrode in alkaline electrolyte.

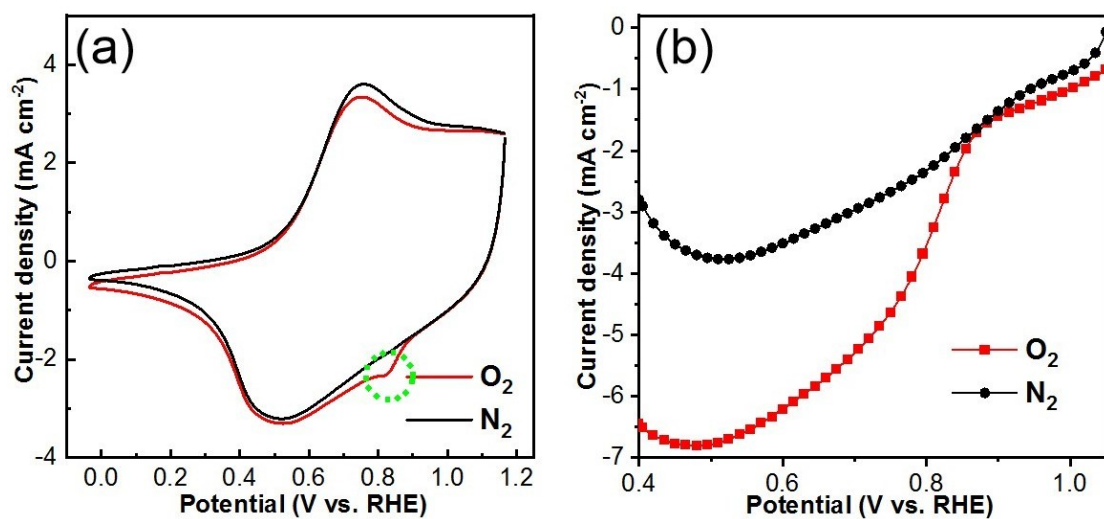


Figure S14. The CV (a) and LSV (b) curves of 5%-Ir-MnO₂ in O₂/N₂-saturated electrolyte.

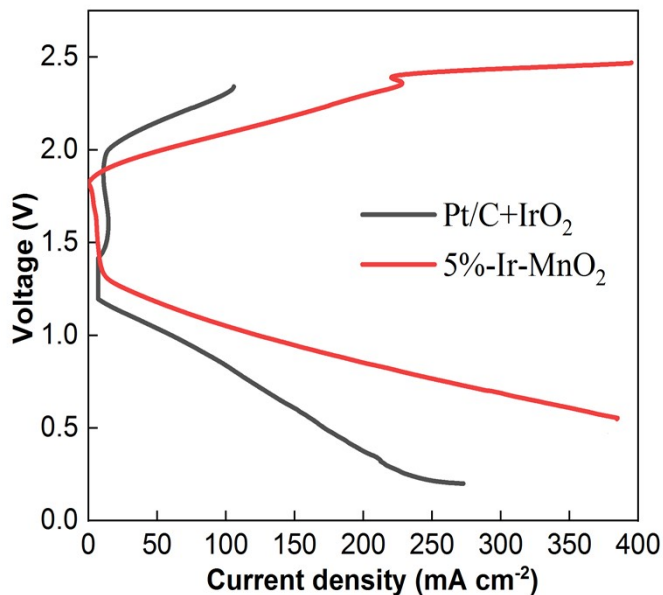


Figure S15. Charge-discharge curves of alkaline Zn-air batteries with 5%-Ir-MnO₂ and Pt/C+IrO₂ as air electrode catalyst.

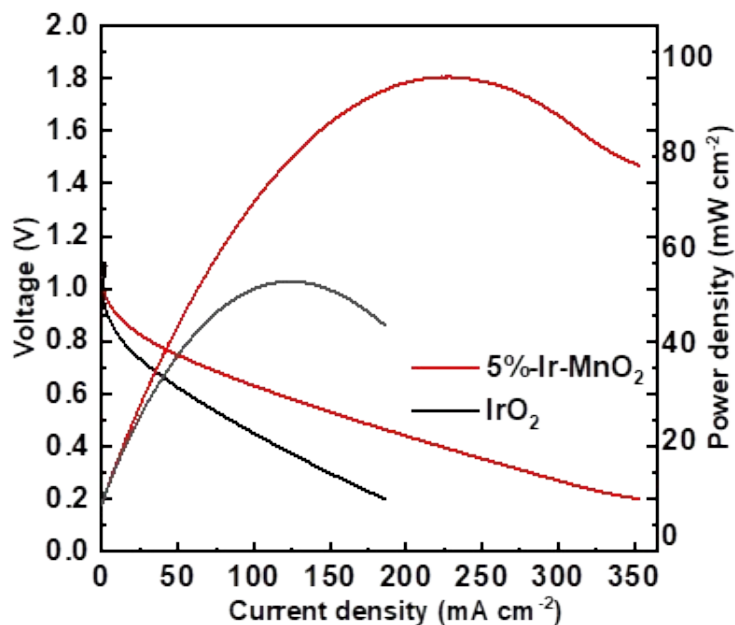


Figure S16. Discharge polarization curve and the corresponding power density of neutral Zn-air batteries with 5%-Ir-MnO₂ and IrO₂ as air electrode catalyst.

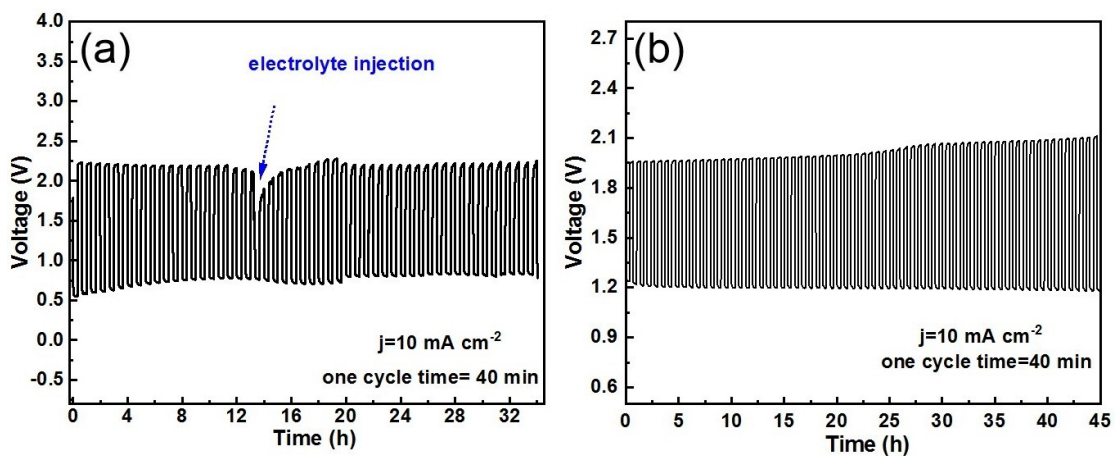


Figure S17. Cycling performance of neutral (a) and alkaline (b) Zn-air battery at 10 mA cm^{-2} and 40 mins for each cycle.

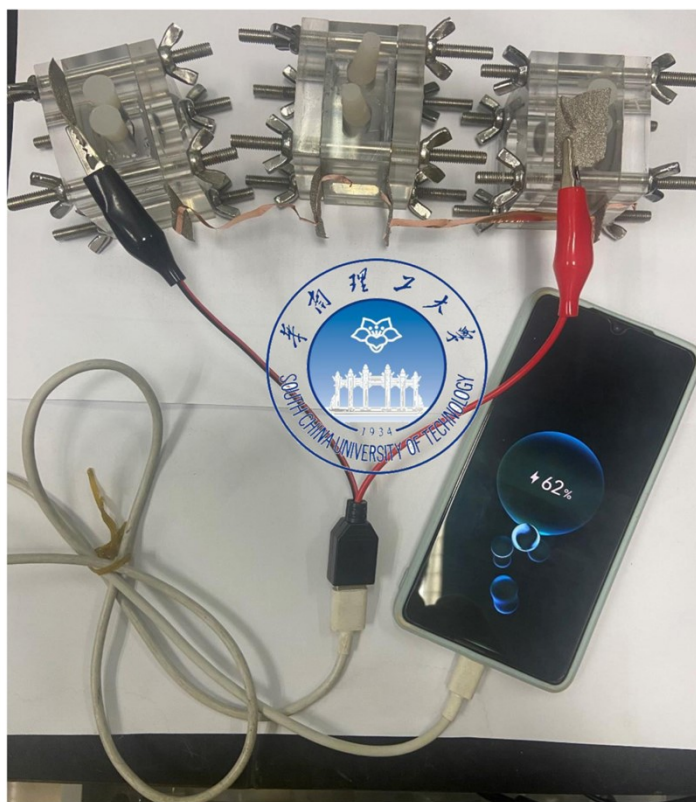


Figure S18. The three alkaline Zn-air batteries in series are charging a mobile phone.

References

1. L. Zhang, L. Wang, Y. Wen, F. Ni, B. Zhang and H. Peng, *Adv. Mater.*, 2020, **32**, 2002297.
2. X. Luo, M. Yang, W. Song, Q. Fang, X. Wei, L. Jiao, W. Xu, Y. Kang, H. Wang, N. Wu, W. Gu, L. Zheng, L. Hu and C. Zhu, *Adv. Funct. Mater.*, 2021, **31**, 2101193.
3. Y. Zhang, C. Wu, H. Jiang, Y. Lin, H. Liu, Q. He, S. Chen, T. Duan and L. Song, *Adv. Mater.*, 2018, **30**, 1707522.
4. C. Wang, P. Zhai, M. Xia, Y. Wu, B. Zhang, Z. Li, L. Ran, J. Gao, X. Zhang, Z. Fan, L. Sun and J. Hou, *Angew. Chem. Int. Ed.*, 2021, **60**, 27126-27134.
5. Y. Zhao, J. Zhang, W. Wu, X. Guo, P. Xiong, H. Liu and G. Wang, *Nano Energy*, 2018, **54**, 129-137.
6. S. Ni, H. Zhang, Y. Zhao, X. Li, Y. Sun, J. Qian, Q. Xu, P. Gao, D. Wu, K. Kato, M. Yamauchi and Y. Sun, *Chem. Eng. J.*, 2019, **366**, 631-638.
7. X. F. Lu, Y. Chen, S. Wang, S. Gao and X. W. Lou, *Adv. Mater.*, 2019, **31**, 1902339.
8. Y. Gu, G. Yan, Y. Lian, P. Qi, Q. Mu, C. Zhang, Z. Deng and Y. Peng, *Energy Stor. Mater.*, 2019, **23**, 252-260.
9. A. Mathur and A. Halder, *Catal. Sci. Technol.*, 2019, **9**, 1245-1254.
10. B. Chen, H. Miao, R. Hu, M. Yin, X. Wu, S. Sun, Q. Wang, S. Li and J. Yuan, *J. Alloys Compd.*, 2021, **852**, 157012.
11. J. Zhang, G. Wang, Z. Liao, P. Zhang, F. Wang, X. Zhuang, E. Zschech and X. Feng, *Nano Energy*, 2017, **40**, 27-33.
12. Q. Shi, C. Zhu, D. Du, J. Wang, H. Xia, M. H. Engelhard, S. Feng and Y. Lin, *J. Mater. Chem. A*, 2018, **6**, 8855-8859.
13. K. Wang, Z. Wang, Y. Liu, J. Liu, Z. Cui, X. Zhang, F. Ciucci and Z. Tang, *Chem. Eng. J.*, 2022, **427**, 131966.